
SN 2023dbc in M108: Optical and Near-Infrared Observations of a Highly-Obscured, Moderately Energetic Stripped-Envelope Supernova

Masayuki Yamanaka¹, Takahiro Nagayama², Akari Kumano³, Devendra Kumar Sahu⁴, Avinash Singh⁵, Hrishav Das⁴, and G. C. Anupama⁴

¹Amanogawa Galaxy Astronomy Research Center (AGARC), Graduate School of Science and Engineering, Kagoshima University, 1-21-35 Korimoto, Kagoshima, Kagoshima 890-0065, Japan

²Graduate School of Science and Engineering, Kagoshima University, 1-21-35 Korimoto, Kagoshima, Kagoshima 890-0065, Japan

³Department of Physics and Astronomy, Faculty of Science, Kagoshima University, 1-21-35 Korimoto, Kagoshima, Kagoshima 890-0065, Japan

⁴Indian Institute of Astrophysics, Koramangala 2nd Block, Bangalore 560034, India

⁵Oskar Klein Centre, Department of Astronomy, Stockholm University, AlbaNova, SE-106 91 Stockholm, Sweden

*E-mail: yamanaka@sci.kagoshima-u.ac.jp

Received (reception date); Accepted (acceptation date)

Abstract

We present near-infrared (NIR) and optical observations of the highly reddened and moderately energetic Type Ib supernova (SN) 2023dbc, covering a period from 2 to 136 days after the explosion. By comparing its color evolution, specifically in $r - JHK_s$ and $i - JHK_s$, with those of broad-lined Type Ic (Ic-BL) and Type IIb SNe, we estimate a significant extinction of $A_V = 4.1 \pm 0.1$ mag toward the SN. The extinction-corrected peak absolute magnitudes are $M_J = -16.8 \pm 0.2$ mag, $M_H = -16.8 \pm 0.2$ mag, and $M_{K_s} = -17.0 \pm 0.2$ mag. The SN exhibited an r -band rise time of 14.9 days. The spectra display broad features indicative of high expansion velocities; the He I line velocity was measured at $16,000 \text{ km s}^{-1}$ at $t = -4$ d. Its spectral profile is broader than those of typical moderately energetic Type Ib SNe, yet narrower than those of Type Ic-BL SNe, placing it in an intermediate category. Based on the light-curve timescale and velocity, we estimate a kinetic energy of $E_k = (4.1 \pm 0.7) \times 10^{51}$ erg, an ejecta mass of $M_{\text{ej}} = 2.3 \pm 0.7 M_{\odot}$, and a radioactive ^{56}Ni mass of $(3.8 \pm 0.1) \times 10^{-2} M_{\odot}$. An analysis using a two-component model suggests a steep density profile in the outer layer contrasted with a dense inner core, which implies ejecta asphericity. The low ^{56}Ni mass is consistent with a partial fallback scenario. We conclude that SN 2023dbc originated from an aspherical explosion with partial core fallback, arising from a progenitor ($M_{\text{ini}} \simeq 15 M_{\odot}$) that had retained its helium envelope within a binary system.

Key words: supernovae: general — supernovae: individual (SN 2023dbc)

1 Introduction

Type Ib/c supernovae (SNe Ib/c) are widely known to be the core-collapse explosions of massive stars that have shed their hydrogen envelopes (Nomoto et al. 1994; Woosley et al. 1995). Specifically, the spectra of SNe Ib **exhibit** helium lines, whereas SNe Ic **lack such features** (Filippenko 1997). However, **because their** progenitors are relatively compact compared to typical supergiants and are often **located** in crowded regions of **their host galaxies** (Anderson & James 2008; Hakobyan et al. 2009; Aramyan et al. 2016), **direct detections** of progenitor stars in pre-explosion images **are** extremely challenging (Cao et al. 2013; Groh et al. 2013; Kilpatrick et al. 2018; Zhao et al. 2025). Consequently, the origin of SNe Ib/c remains a highly **debated** and unresolved **issue in stellar astrophysics**.

Light curve and spectral analyses of SNe Ib/c **have revealed** low ejecta masses and typical kinetic energies (Cano 2013; Prentice et al. 2016; Lyman et al. 2016). These results support the **hypothesis** that the progenitors may **originate** from low-mass stripped-envelope stars, **rather** than from very massive stars (Hachinger et al. 2012; Dessart et al. 2020). Such low-mass progenitors are **well** reproduced by binary interaction scenarios (Yoon et al. 2010; Dessart et al. 2012; Tauris et al. 2015). On the other hand, some highly energetic events are often associated with intense high-energy emission **such as** gamma-ray **bursts** (Galama et al. 1998; Stanek et al. 2003; Malesani et al. 2004). The progenitors of these events are **suggested** to be Wolf–Rayet stars that evolved from massive stars with initial masses $> 25 M_{\odot}$ (Iwamoto et al. 1998; Iwamoto et al. 2000; Mazzali et al. 2003). The event rate of SNe Ib/c obtained **from** volume-limited **samples** is approximately **one-third** of that of SNe II (Li et al. 2011; Graur et al. 2017; Ma et al. 2025). Therefore, a **larger number of** well-observed nearby samples is **essential** for a comprehensive understanding.

Given the crowded environments of their explosion sites, some SNe Ib/c are discovered within the spiral arms of their host galaxies. Consequently, they are often affected by significant extinction due to interstellar dust (Kankare et al. 2014b; Kankare et al. 2014a; Jencson et al. 2017; Jencson et al. 2018; Kool et al. 2018; Kankare et al. 2021). The intrinsic SN event rate in dusty environments remains uncertain (Mattila et al. 2012), and investigating such highly obscured events would enhance our understanding of the properties of these phenomena. Although follow-up observations of these highly reddened SNe are challenging at optical

wavelengths, NIR observations are less affected because scattering and absorption are much weaker. However, the number of facilities capable of such NIR monitoring has been limited.

SN 2023dbc was discovered at $r = 19.5$ mag in a spiral arm of the galaxy M108 on 2023 March 13 at 06:53:43 UT (Ho 2023) by the Zwicky Transient Facility (ZTF; Bellm et al. 2019). **Remarkably**, the last non-detection limit was recorded at $r = 20.3$ mag **only** 40 minutes prior, on 2023 March 13 at 06:16:42 UT (Ho 2023). **Subsequent** independent detection was provided by the Asteroid Terrestrial-impact Last Alert System (ATLAS; Tonry et al. 2018), **which reported** $o = 17.5$ mag on 2023 March 16 at 10:54:10 UT. The corresponding non-detection limit was $o = 19.2$ mag on 2023 March 12 at 11:34:41 UT, approximately eighteen hours before the ZTF discovery. **Additionally, we obtained forced photometry data from the ATLAS server** (Smith et al. 2020; Shingles et al. 2021) **to further constrain the early-phase light curve.**

Following the discovery, spectroscopic identification was **carried out**. The object was initially classified as a young Type II SN on March 16 **based on a spectrum obtained with the Lijiang-2.4m/YFOSC** (Li et al. 2023). However, a **subsequent** spectrum obtained with Keck-I/LRIS (Perley et al. 2023) identified the object as a highly reddened Type Ic SN **in its early phases. In this study, through our detailed multi-band light curve and spectroscopic analyses, we finally identify SN 2023dbc as a Type Ib SN, characterized by the presence of prominent He I lines.**

The remainder of this paper is organized as follows. In §2, we describe the observations and data reduction procedures in detail. Section 3 presents the results of our photometric and spectroscopic analyses, while we discuss the **derived** ejecta and progenitor properties in §4. Finally, we summarize our findings and **conclude the study** in §5.

2 Observations and Data reduction

NIR JHK_s -band photometric observations were **obtained over 17 nights** between 2023 March 15.6 and July 17.5 using the kSIRIUS instrument **mounted at the Cassegrain focus** of the 1-m telescope at Kagoshima University (Nagayama & Nakaya 2024). Optical *griz*-band observations **were collected on 7 nights from March 19.6 to April 13.9** using the GROWTH-India Telescope (GIT; Kumar et al. 2022). In addition, publicly available optical *g*- and *r*-band data from the Zwicky Transient Facility (ZTF; Bellm et al. 2019) and *o*-band

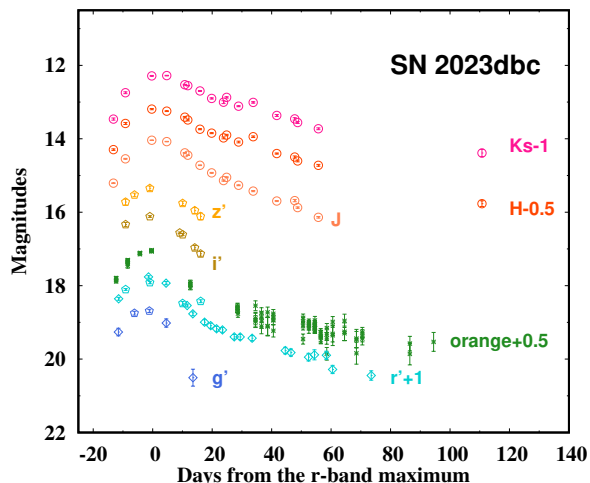


Fig. 1. Optical and NIR g' , r' , o , i , z , J , H , and K_s -band light curves of SN 2023dbc. Note that these light curves have not been corrected for Galactic or host-galaxy extinction. For clarity, the data are plotted with arbitrary vertical offsets. The g' , r' , o , i , and z -band magnitudes are presented in the AB system, whereas the J , H , and K_s magnitudes are in the Vega system. The r -band maximum date is adopted as the reference epoch ($t = 0$). Alt text: The horizontal axis represents the phase in days relative to the r -band maximum light.

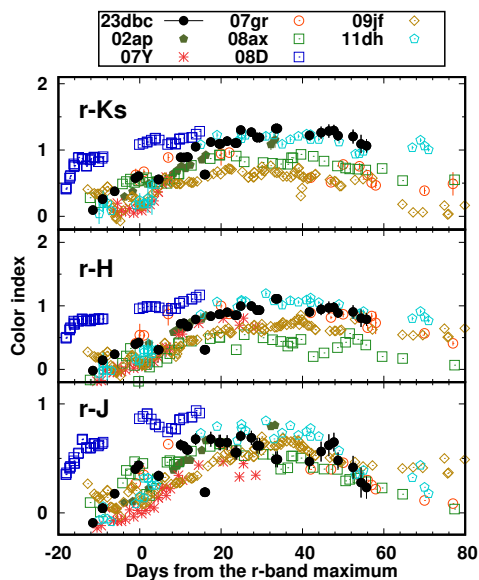


Fig. 2. Extinction-corrected $r - K_s$, $r - H$, and $r - J$ color evolutions of SN 2023dbc. These are compared with those of SNe 2002ap (Yoshii et al. 2003; Tomita et al. 2006), 2007Y (Stritzinger et al. 2009), 2007gr (Hunter et al. 2009), 2008D (Modjaz et al. 2009; Bianco et al. 2014), 2008ax (Pastorello et al. 2008; Bianco et al. 2014), 2009jf (Sahu et al. 2011; Valenti et al. 2011; Bianco et al. 2014), and 2011dh (Sahu et al. 2013; Ergon et al. 2014; Marion et al. 2014). Note that $R - K_s$, $R - H$, and $R - J$ are plotted for the comparison. The color evolution of SN 2011dh were adopted as a template to derive the color excesses for SN 2023dbc: $E(r - K_s) = 2.9$, $E(r - H) = 2.7$, and $E(r - J) = 2.3$. These values were applied to correct the observed colors of SN 2023dbc. Alt text: Three line graphs showing color evolution. The horizontal axis represents the phase in days relative to the maximum light.

data from the Asteroid Terrestrial-impact Last Alert System (ATLAS; Tonry et al. 2018) were integrated into the analysis.

Data reduction for the kSIRIUS and GIT imaging data was performed through a standard procedure. After initial preprocessing, we performed point-spread function (PSF) fitting photometry on all images. Photometric calibration for the SN and reference stars was calibrated against the Pan-STARRS (Chambers et al. 2016) and 2MASS (Cutri et al. 2003) catalogues for the optical and NIR data, respectively. The resulting multi-band light curves are presented in Figure 1.

Spectroscopic observation was conducted on 2023 March 24 using the Himalayan Faint Object Spectrograph and Camera (HFOSC), mounted on the 2-m Himalayan Chandra Telescope (HCT) at the Indian Astronomical Observatory (IAO), Hanle, India. A slit width of $1''.92$ and the Grism 7 (gr7) were employed for the observation. A blue spectrophotometric standard star was also observed on the same night for flux calibration. Data reduction followed standard IRAF-based procedures (or other software if applicable). Wavelength calibration was performed using a FeAr arc lamp, and flux calibration was achieved using the aforementioned standard star. We also incorporated an additional spectrum retrieved from the TNS public database. The wavelengths of these spectra were corrected to the rest frame adopting a redshift of $z = 0.0023$ (Springob et al. 2005). To determine the He I line velocity, we measured the absorption minimum by fitting a Gaussian function, where the measurement error was estimated to be $\sim 210 \text{ km s}^{-1}$.

3 Results

3.1 Distance and extinction

The host galaxy M108 is a nearby system located at a low redshift. Given the large scatter among the distance estimates derived from various methods and the lack of Cepheid-based calibration, we adopted a distance of $9.9 \pm 0.7 \text{ Mpc}$ for the host galaxy. This value is based on the average of Tully–Fisher relation measurements reported in the literature (Bottinelli et al. 1985; Bottinelli et al. 1984; Bottinelli et al. 1986; de Vaucouleurs et al. 1981; Giraud 1985; Nasonova et al. 2011; Kashibadze 2008; Sorce et al. 2014a; Tully et al. 2016; Sorce et al. 2014b; Karachentsev et al. 2013; Tully et al. 2013; Tully et al. 2009; Springob et al. 2009; Tully & Fisher 1988; Karachentsev et al. 2006; Tully et al. 1992).

First, we accounted for Galactic extinction ($A_V = 0.05 \text{ mag}$) using the dust extinction maps of

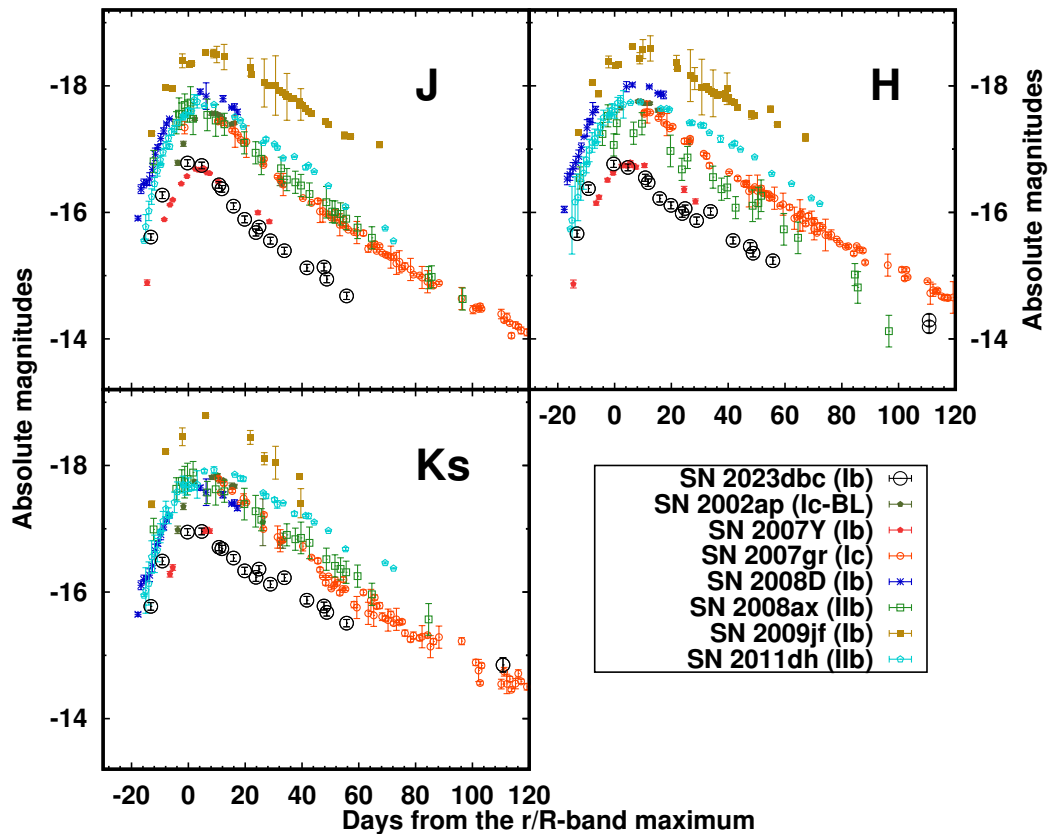


Fig. 3. NIR J , H , and K_s -band absolute magnitude light curves of SN 2023dbc, compared with those of other SNe Ib/c and IIb. The light curves were corrected for extinction using $A_J = 1.0$, $A_H = 0.7$, and $A_{K_s} = 0.4$ mag, assuming a distance modulus of $\mu = 29.8$ mag. For SN 2023dbc, the reference epoch ($t=0$) is the date of the r -band maximum, whereas for the comparison objects, the reference epochs are as defined in their respective literature. Alt text: Three panels showing absolute magnitude evolution. The horizontal axis represents the phase in days relative to the maximum light.

Schlafly & Finkbeiner (2011). Regarding the host-galaxy extinction, the equivalent-width method using Na I D absorption lines could not be applied due to the low signal-to-noise (S/N) ratio of our optical spectra. Therefore, we relied on a template color-evolution comparison for the extinction correction. The $r-J$, $r-H$, and $r-K_s$ color evolutions were compared with those of other Type Ib, Ic, and IIb SNe (Figure 2), where the comparison samples were corrected for extinction according to their respective references. We found that the color evolutions of SN 2023dbc are remarkably consistent with those of the Type IIb SN 2011dh, as well as the broad-lined Type Ic SN 2002ap.

In contrast, the $r-K_s$ and $r-H$ color evolutions of the other SNe in our sample are relatively constant. Based on these comparisons, we adopted the color evolutions of SNe 2011dh and

2002ap as templates for our extinction estimation. We determined the color excesses to be $E(r-J) = 2.27 \pm 0.12$ mag, $E(r-H) = 2.56 \pm 0.08$ mag, and $E(r-K_s) = 2.94 \pm 0.07$ mag. By assuming the standard Galactic extinction law with $R_V = 3.1$ (Cardelli et al. 1989), these values yield a total visual extinction of $A_V = 4.07 \pm 0.07$ mag.

Using a similar approach, we also estimated the extinction using $i-J$, $i-H$, and $i-K_s$ color templates, which yielded color excesses of $E(i-J) = 1.51 \pm 0.09$ mag, $E(i-H) = 1.85 \pm 0.06$ mag, and $E(i-K_s) = 2.15 \pm 0.14$ mag. These values lead to $A_V = 4.05 \pm 0.09$ mag, which is highly consistent with the results derived from the $r-JHK_s$ templates. Therefore, we adopt $A_V = 4.1 \pm 0.1$ mag as the host-galaxy extinction throughout this paper.

Alternatively, we cross-checked the extinction value using the optical spectrum. First,

we performed template fitting with GELATO (Harutyunyan et al. 2008) while varying the reddening as a free parameter. The fit quality remained high for $E(B - V)$ in the range of 1.0–1.3 mag; the latter value is consistent with the extinction derived from our color-template analysis ($A_V = 4.1$ mag). To further confirm both the classification and reddening, we employed SNID-SAGE (Stoppa & Smartt 2026), which showed an excellent match with the broad-lined Type Ic (SN Ic-BL) PTF10vgv. These results demonstrate that the optical spectral features are consistent with those of an SN Ic-BL, and the overall spectral slope is fully compatible with the high extinction ($A_V = 4.1$ mag) determined above.

3.2 Light curves

The g, r, o, J, H , and K_s -band light curves are shown in Figure 1. We performed polynomial fitting to the r, o, J, H , and K_s -band light curves to estimate their peak magnitudes and epochs of maximum light. The resulting maximum magnitudes are 16.8, 16.5, 13.9, 13.6, and 13.2 mag, which were reached on MJD 60032.8, 60030.6, 60031.2, 60031.1, and 60031.1, respectively. We define the epoch of the r -band maximum as $t = 0$ throughout this paper.

To constrain the explosion epoch, we performed a fit to the rising phase of the r and o -band light curves using a modified exponential function. The fit yielded an estimated explosion date of MJD 60017.6. Independently, we constrained the explosion date to $\text{MJD } 60017.85 \pm 0.75$ (or simply MJD 60017.85) based on the midpoint between the first discovery and the last non-detection epochs. This result is highly consistent with the value obtained from the light-curve fitting. Therefore, we adopt a rise time of 14.9 days throughout this paper.

We obtained the $rJHK_s$ -band absolute magnitudes of SN 2023dbc by correcting for the Galactic (Schlafly & Finkbeiner 2011) and host-galaxy extinctions ($A_V = 4.1$; see § 3.1), assuming a distance modulus of $\mu = 29.8$. The peak absolute magnitudes were determined to be $M_r = -16.3 \pm 0.2$ mag, $M_J = -16.8 \pm 0.2$ mag, $M_H = -16.8 \pm 0.2$ mag, and $M_{K_s} = -17.0 \pm 0.2$ mag. The J, H , and K_s -band light curves are compared with those of other SNe Ib, Ic, and Ic-BL in Figure 3. The absolute magnitudes of SN 2023dbc lie at the faint end of the distribution for these SNe, but are broadly comparable to those of typical SNe Ib/c. After the maximum, the decline rates of SN 2023dbc are consistent with those of the comparison.

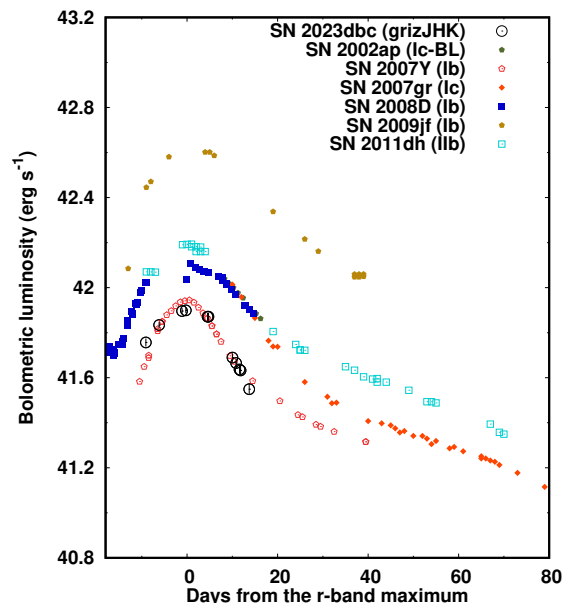


Fig. 4. Quasi-bolometric light curve of SN 2023dbc, derived by integrating the g, r, i, z, J, H , and K_s -band photometric data. For comparison, the bolometric light curves of other SNe are also shown, including SNe 2002ap (Foley et al. 2003; Yoshii et al. 2003; Tomita et al. 2006), 2007Y (Stritzinger et al. 2009), 2007gr (Valenti et al. 2008b; Hunter et al. 2009), 2008D (Modjaz et al. 2009), 2009jf (Valenti et al. 2011), and 2011dh (Ergon et al. 2014), which were constructed from $BVRIZJK_s$ -band data. All text: The vertical and horizontal axes represent the luminosity in erg s^{-1} and the phase in days relative to maximum light, respectively.

SN 2007Y is another example of an intrinsically faint Type Ib SN, with a peak V -band absolute magnitude of $M_V = -16.5$ mag (Stritzinger et al. 2009). Considering the uncertainties in both extinction and distance, its luminosity is comparable to that of SN 2023dbc. However, as will be discussed in § 3.4, their spectral features exhibit significant differences.

3.3 Bolometric light curves

The quasi-bolometric light curve was constructed by integrating the flux densities at the effective wavelengths of each filter (Fukugita et al. 1996), assuming linear interpolation between the data points. We utilized the g, r, i, z, J, H , and K_s -band fluxes, which were derived from the observed magnitudes after correcting for the extinction of $A_V = 4.1$ mag (see § 3.1) and adopting the distance to the host galaxy M108. Following Lyman et al. (2014), we assumed that the $grizJHK_s$ bands cover approximately 80% of the total bolometric flux. The resulting quasi-bolometric light curve is shown in Figure 4. The peak bolometric luminosity was estimated to be $\sim 5.8 \times 10^{41} \text{ erg s}^{-1}$.

The quasi-bolometric light curves were compared

with other stripped-envelope SNe, including SNe 2002ap (Foley et al. 2003; Yoshii et al. 2003; Tomita et al. 2006), 2007Y (Stritzinger et al. 2009), 2007gr (Valenti et al. 2008b; Hunter et al. 2009), 2008D (Modjaz et al. 2009), 2009jf (Valenti et al. 2011; Sahu et al. 2011), and 2011dh (Ergon et al. 2014). For these objects, we accounted for distance and extinction using values reported in the literature. The fraction of the $BVRIJHK_s$ -band flux to the total bolometric flux for this comparison sample was also assumed to be $\sim 80\%$, the same as that used for SN 2023dbc.

The peak luminosity of SN 2023dbc was significantly lower than those of other SNe Ib, Ic, and Ic-BL. SN 2007Y is recognized as one of the faintest Type Ib SNe within the sample studied by Lyman et al. (2016). Notably, even after accounting for the uncertainties in distance and extinction, the luminosity of SN 2023dbc remains remarkably low, appearing even fainter than that of SN 2007Y.

The peak luminosity of stripped-envelope SNe is primarily determined by the radioactive ^{56}Ni mass and the rise time (Arnett 1982). Using a rise time of 14.9 days and the peak luminosity derived above, the radioactive ^{56}Ni mass was estimated to be $(3.8 \pm 0.1) \times 10^{-2} M_{\odot}$. This mass lies at the lower edge of the distribution for SNe Ib/c and Ic-BL (Lyman et al. 2016; Afsariardchi et al. 2021). Specifically, it is smaller than the ^{56}Ni masses reported for the SN Ic-BL 2002ap ($0.07 M_{\odot}$; Mazzali et al. 2002) and the SN Ib 2007Y ($0.06 M_{\odot}$; Stritzinger et al. 2009).

3.4 Spectra

Figure 5 shows the spectral evolution of SN 2023dbc. Although the observed spectra are significantly reddened owing to the high extinction, several absorption features can be clearly identified. Specifically, the He I $\lambda 5876$, $\lambda 6678$, and $\lambda 7065$ lines are present. The Si II $\lambda 6355$ absorption feature is also visible around $t = 4$ d. For the subsequent analysis, these spectra were corrected for extinction using $A_V = 4.1$ mag, assuming the standard reddening law with $R_V = 3.1$.

In Figure 6, the extinction-corrected spectrum is compared with those of the well-studied Type Ib SN 2012au (Takaki et al. 2013) and the SNe Ic-BL 2002ap (Kinugasa et al. 2002; Foley et al. 2003) and 2003jd (Valenti et al. 2008a). Compared to SN 2012au, the absorption lines in SN 2023dbc appear broader and more blended. The blueshifted O I $\lambda 7774$ absorption feature is clearly identified, indicating an expansion velocity higher than

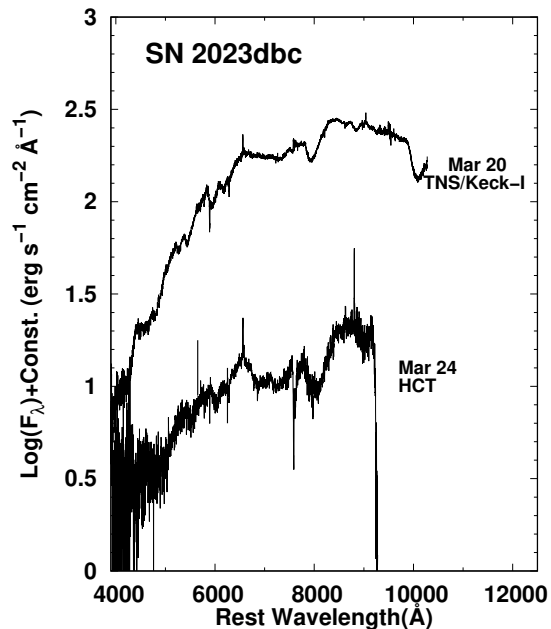


Fig. 5. Optical spectra of SN 2023dbc obtained at $t = -8$ d and $t = -4$ d relative to the r -band maximum. The spectra are shown without correction for extinction. Alt text: The vertical axis represents the flux density in units of $\text{erg s}^{-1} \text{cm}^{-2} \text{\AA}^{-1}$ on a logarithmic scale, and the horizontal axis represents the observed wavelength in \AA .

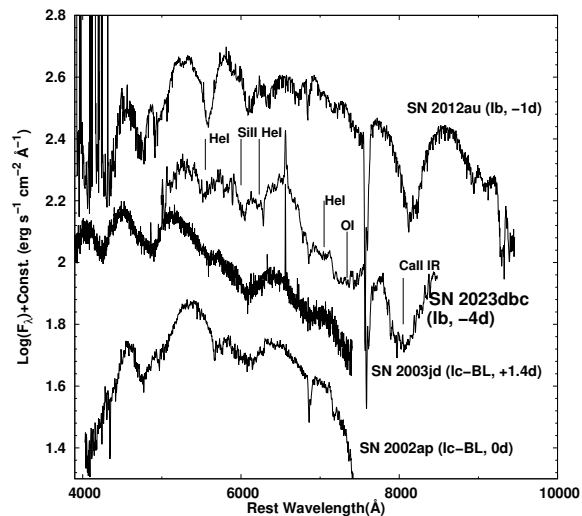


Fig. 6. Extinction-corrected spectrum of SN 2023dbc ($A_V = 4.1$ mag and $R_V = 3.1$). The spectrum was smoothed using a 5-pixel boxcar window to enhance the signal-to-noise ratio. For comparison, spectra of the Type Ic-BL SNe 2002ap, 2003jd (Valenti et al. 2008a), and the Type Ib SN 2012au (Takaki et al. 2013) are also shown. The $t = 0$ d spectrum of SN 2002ap was retrieved from the Weizmann Interactive Supernova data Repository (WiSeREP; Yaron & Gal-Yam 2012) with original data reported in Foley et al. (2003) and Kinugasa et al. (2002). All wavelengths have been shifted to the rest frame using the recession velocity of each host galaxy. Alt text: The vertical axis represents the flux density on a logarithmic scale, and the horizontal axis represents the rest-frame wavelength.

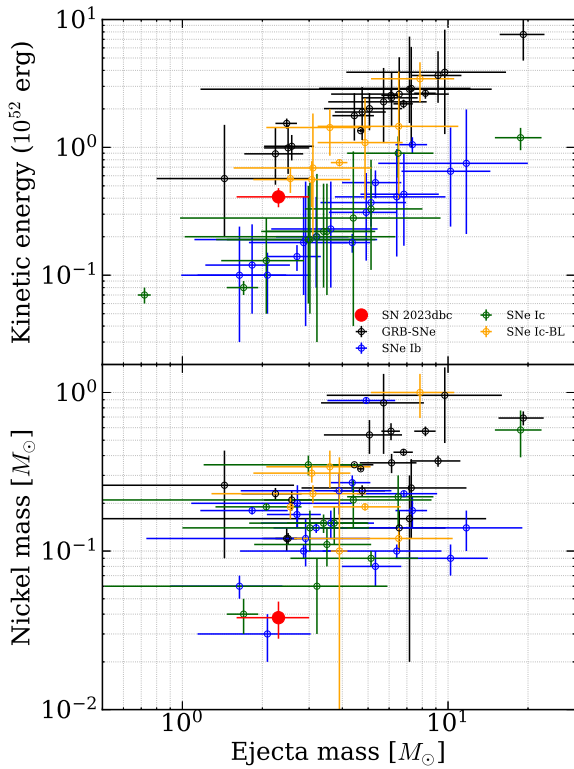


Fig. 7. (Upper panel) Ejecta mass (M_{ej}) versus kinetic energy (E_{kin}) for SN 2023dbc compared with the large sample from Cano (2013). The explosion properties of SN 2023dbc are consistent with those of typical SNe Ib/c. (Lower panel) Similar to the upper panel, but showing the correlation between M_{ej} and the radioactive ^{56}Ni mass (M_{Ni}). In both panels, SN 2023dbc is located within the distribution of standard stripped-envelope SNe. All text: The vertical axis shows the kinetic energy in logarithmic scale, in units of erg in upper panel, and the nickel mass in logarithmic scale, in units of solar mass in lower panel. The horizontal axis shows the ejecta mass in logarithmic scale, in units of solar mass.

that of SN 2012au. Furthermore, the Ca II NIR triplet exhibits a significantly higher velocity than that observed in SN 2012au.

While the overall spectral profile resembles that of the Type Ic-BL SN 2003jd, the He I $\lambda 5876$, $\lambda 6678$, and $\lambda 7065$ absorption features are distinctly visible in SN 2023dbc. Notably, the absorption features of Si II $\lambda 6355$ and He I $\lambda 6678$ are marginally resolved; in contrast, these features are typically blended in SNe Ic-BL because of their significantly higher expansion velocities.

4 Discussion

The ejecta mass (M_{ej}) and kinetic energy (E_{kin}) are fundamentally related to the opacity (κ), the diffusion timescale (τ_{diff}), and the expansion velocity (v) of the supernova ejecta (Arnett 1982). These relationships are governed by the following scaling laws:

$$\tau_{\text{diff}} \propto \kappa^{1/2} M_{\text{ej}}^{3/4} E_{\text{kin}}^{-1/4}, \quad (1)$$

$$v \propto M_{\text{ej}}^{-1/2} E_{\text{kin}}^{1/2}. \quad (2)$$

We adopt the observed rise time ($\tau_{\text{rise}} = 14.9$ days) as a proxy for the diffusion timescale. The expansion velocity was measured to be $v = 16,000 \text{ km s}^{-1}$ using the spectrum at $t = -4$ d; however, the line velocities exhibit a rapid decline during this phase. Assuming a decline rate of $500 \text{ km s}^{-1} \text{ d}^{-1}$ (e.g., Sahu et al. 2011), the velocity at $t = 0$ d is inferred to be $v \approx 14,000 \text{ km s}^{-1}$. We use this value to estimate the physical properties of the ejecta.

Since the absolute value of κ is model-dependent, we employ a relative scaling method to mitigate this uncertainty, using SN 2012au as a reference. For SN 2012au, Takaki et al. (2013) reported a He I line velocity of $13,500 \text{ km s}^{-1}$ and a rise time of 16.3 days, corresponding to $M_{\text{ej}} = 6.5 M_{\odot}$ and $E_{\text{kin}} = 5.1 \times 10^{51} \text{ erg}$. By applying the scaling laws, we obtain the explosion properties for SN 2023dbc as $M_{\text{ej}} = 7.1 \pm 1.4 M_{\odot}$ and $E_{\text{kin}} = (5.7 \pm 3.2) \times 10^{51} \text{ erg}$.

We also independently estimated the ejecta mass as $M_{\text{ej}} = 1.6 \pm 0.3 M_{\odot}$ and the kinetic energy as $E_{\text{kin}} = (1.6 \pm 0.9) \times 10^{51} \text{ erg}$, based on the scaling-law method using the reference values for the energetic Type Ic-BL SN 2002ap from Lyman et al. (2016). For this calibration, we adopted a reference velocity of $13,000 \text{ km s}^{-1}$ and a rise time of 12.45 days for SN 2002ap. These results are notably lower than our initial estimates derived from SN 2012au. This discrepancy likely arises from differences in the assumed model parameters and coefficients, such as the optical opacity (κ_{opt}), adopted in different studies. By combining these two independent calibrations, we aimed to account for the systematic uncertainties arising from different model assumptions, such as the opacity and ejecta structure inherent in each study. Consequently, we obtained $M_{\text{ej}} = 4.4 \pm 2.8 M_{\odot}$ and $E_{\text{kin}} = (3.7 \pm 2.1) \times 10^{51} \text{ erg}$ as our final estimates for SN 2023dbc.

Cano (2013) also presented an analytic investigation of a collected sample of Type Ib, Ic, Ic-BL, and GRB-SNe. Figure 7 shows the kinetic energy plotted against the ejecta mass for SN 2023dbc, along with the sample from Cano (2013). Our derived explosion properties are consistent with the distribution of SNe Ic-BL, although both parameters are located toward the lower end of the population. This finding is consistent with the overall spectral profile, which exhibits the broad features characteristic of moderately energetic events.

Mazzali et al. (2007) discussed the possibility of an as-

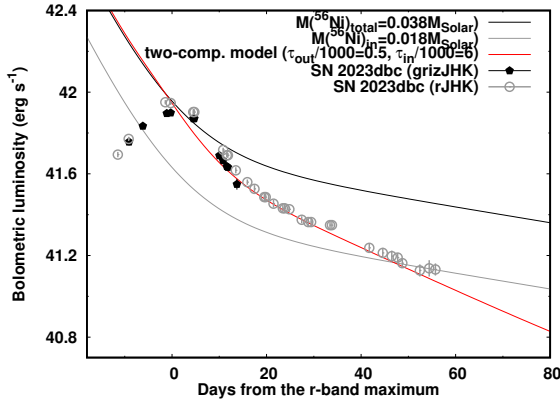


Fig. 8. Quasi-bolometric light curve of SN 2023dbc. In addition to the flux integrated over the *grizJHK_s* bands, the curve derived from the integration of *rJHK_s* data is also shown for comparison. The data are fitted with two-component model curves (Maeda et al. 2003) characterized by γ -ray optical depths of $\tau_{\text{out}}/1000 = 0.5$ and $\tau_{\text{in}}/1000 = 6$. The model assumes an outer-layer ^{56}Ni mass of $M(^{56}\text{Ni})_{\text{out}} = 0.02 M_{\odot}$ and an inner-layer mass of $M(^{56}\text{Ni})_{\text{in}} = 0.018 M_{\odot}$. The total synthesized ^{56}Ni mass adopted for this two-component model is $M(^{56}\text{Ni})_{\text{total}} = (3.8 \pm 0.1) \times 10^{-2} M_{\odot}$. Alt text: The vertical axis is scaled in erg per second. The horizontal axis is scaled in days from the maximum light.

pherical explosion scenario based on a theoretical analysis of the line profiles in the nebular-phase spectra of the faint Type Ic-BL SN 2002ap. To investigate this further, we calculated two-component model light curves following the methodology described in Maeda et al. (2003). In this model, the ejecta structure is assumed to consist of an outer layer with low density and a high-density inner core. The model parameters are described as follows:

$$L_{\text{bol}} = M(^{56}\text{Ni})_{\text{in}} e^{-t_d/113} [\epsilon_{\gamma}(1 - e^{-\tau_{\text{in}}}) + \epsilon_{e+}] + M(^{56}\text{Ni})_{\text{out}} e^{-t_d/113} [\epsilon_{\gamma}(1 - e^{-\tau_{\text{out}}}) + \epsilon_{e+}] \quad (3)$$

To demonstrate the applicability of this model, we constructed the quasi-bolometric light curve of SN 2023dbc by integrating the flux using only the *r*, *J*, *H*, and *K_s*-band data up to $t \approx 60$ d, following the method described in § 3. For this specific calculation, the ratio of the *rJHK_s* integrated flux to the total bolometric flux is assumed to be $\sim 80\%$. We performed a fit of the model light curve to the observations (see Figure 8). To reproduce the observed light curve, the outer-layer ejecta require a γ -ray optical depth of $\tau_{\text{out}}/1000 \approx 0.5$, while the inner core requires $\tau_{\text{in}}/1000 \approx 6$. The significant ratio of $\tau_{\text{in}}/\tau_{\text{out}} = 12$ is indicative of a steep density gradient between the outer ejecta and the high-density core. This trend is consistent with the results reported for the highly energetic SNe 1998bw and 2002ap (Maeda et al. 2003).

Considering the similarity with these SNe, an aspherical ejecta structure is strongly suggested. In this asymmetric configuration, relatively high-velocity ejecta are expected to be rich in ^{56}Ni along the jet axis, while a ring-like geometry of oxygen-rich gas is expected in the equatorial plane (Maeda et al. 2008). If the viewing angle is off-axis (e.g., perpendicular to the jet), a more moderate energy would be observed compared to the on-axis direction. This scenario is consistent with the picture of a bipolar explosion, albeit less extreme than prominent cases such as SN 2008D (Tanaka et al. 2009a).

Alternatively, we consider a fallback scenario in which the inner part of the ejecta accretes onto the central remnant, such as a black hole. In this case, the newly synthesized elements in the inner region, including a significant fraction of the radioactive ^{56}Ni , would be sequestered into the central object. Another possibility is a low-energy explosion, resulting in a very small synthesized ^{56}Ni mass (e.g., $< 0.01 M_{\odot}$), as seen in extremely faint SNe IIP (Turatto et al. 1998; Zampieri et al. 2003). However, the radioactive ^{56}Ni mass of SN 2023dbc is $\approx 3.8 \times 10^{-2} M_{\odot}$, which is larger than typical values predicted by simple fallback scenarios. In such scenarios, the ejecta mass is expected to be large while the total explosion energy remains small, which contrasts with the moderately large kinetic energy and ejecta mass derived for SN 2023dbc. These arguments suggest that a partial fallback of the inner core may have occurred. The inferred weak asphericity of the ejecta structure supports this fallback mechanism, where the inner core is relatively dense, but not significantly denser than those of SNe 1998bw and 2002ap. Based on these considerations, an aspherical explosion scenario involving the formation of a central black hole is consistent with the observed properties of SN 2023dbc, although further analysis of late-phase data is needed to confirm this picture.

The ratio of $M(^{56}\text{Ni})_{\text{in}}/M(^{56}\text{Ni})_{\text{out}} \approx 0.9$ is larger than those observed in highly energetic SNe such as SNe 1998bw and 2002ap (Maeda et al. 2003). This is consistent with a degree of moderate ejecta mixing. Such moderate mixing, often linked to an asymmetric explosion, may contribute to the formation of He I absorption lines (Cano et al. 2014). The absorption features of He I $\lambda 5876$, $\lambda 6678$, and $\lambda 7065$ are typically produced by non-thermal excitation driven by the radioactive decay of ^{56}Ni (Hachinger et al. 2012). While SNe Ic-BL occasionally exhibit these He I lines due to this mechanism, SN 2023dbc appears to be a transitional object between normal SNe Ib and SNe Ic-BL. Furthermore, the short rise time observed for SN 2023dbc is consistent with

a **significant fraction** of ^{56}Ni being distributed in the outer **layers** of the ejecta.

Based on the **estimated** total ejecta mass of $M_{\text{ej}} \approx 2.3 M_{\odot}$ and assuming the $M_{\alpha}-M_{\text{MS}}$ relation (Sugimoto & Nomoto 1980), the main-sequence mass of the progenitor is estimated to be $M_{\text{MS}} \approx 15 M_{\odot}$. This initial mass is consistent with the progenitors of **normal** SNe Ib/c, such as SN 1994I (Nomoto et al. 1994), but is **notably** smaller than the estimates for SNe 2008D (Tanaka et al. 2009b) and 2002ap (Mazzali et al. 2002; Mazzali et al. 2007). Generally, the hydrogen envelope of a massive star is **effectively** stripped by radiation-driven winds for **very massive stars** (Castor et al. 1975). **However, for SN 2023dbc, whose** ejecta mass is comparable to typical SNe **despite a relatively small** ^{56}Ni mass, **binary interaction may be required to sufficiently** strip the envelope. **Taken together,** these arguments suggest that SN 2023dbc **originated** from an aspherical explosion with **partial fallback, resulting from a moderate-mass** progenitor in a binary system.

5 Conclusion

SN 2023dbc is a highly reddened Type Ib SN, characterized by a relatively faint intrinsic peak **luminosity**, a fast rise time, and **high-velocity HeI absorption features**. Based on these observational properties, we **estimated** the explosion parameters of this object. The faint peak and short rise time constrain the ejected ^{56}Ni mass to a relatively low value of $M(^{56}\text{Ni}) = (3.8 \pm 0.1) \times 10^{-2} M_{\odot}$. Furthermore, the high expansion velocity and short characteristic timescale yield **an** ejecta mass of $M_{\text{ej}} = 2.3 \pm 0.7 M_{\odot}$ and a kinetic energy of $E_{\text{kin}} = (4.1 \pm 0.7) \times 10^{51}$ erg. The **relatively small ratio of the synthesized** ^{56}Ni mass to the ejecta mass is consistent with the explosion **models proposed for** the intrinsically faint **Type Ic-BL** SN 2002ap.

The analysis **using** the two-component model **demonstrates** that the density profile is steep in the outer **layers** while **maintaining** a dense inner core. This structure **suggests an aspherical explosion geometry, albeit one that is less pronounced** than that of SN 2002ap. The short rise time **further supports the presence of** moderate mixing **within** the ejecta. The **relatively low** ^{56}Ni mass is **well-explained** by a partial fallback scenario, **which** is consistent with the hypothesis that **the SN was observed from a direction almost perpendicular to the high-velocity (jet-like) ejecta**. This **configuration** is similar to the **off-axis view proposed for the aspherical explosion structure of SN 1998bw** (Maeda et al. 2008).

The relatively **small** ejecta mass indicates that the **zero-age main-sequence mass** of the progenitor was likely $M_{\text{ZAMS}} \approx 15 M_{\odot}$. The progenitor **was presumably** stripped of its hydrogen envelope **via** binary interaction, **leaving a helium star as the pre-supernova progenitor**. This suggests that SN 2023dbc resulted from an aspherical explosion **associated with the partial fallback of the inner core onto a black hole, originating** from a moderately massive star in a close binary system.

Acknowledgments

We are grateful to graduate and undergraduate students for performing the near-infrared observations. This work was supported by Grant-in-Aid for Scientific Research (C) 22K03676. The Kagoshima University 1 m telescope is a member of the Optical and Infrared Synergetic Telescopes for Education and Research (OISTER) program funded by the MEXT of Japan. This work was supported by JSPS Bilateral Program Number JPJSBP 120227709. The GROWTH-India Telescope (GIT) is a 70-cm telescope with a $0^{\circ}.7$ field of view, set up by the Indian Institute of Astrophysics (IIA) and the Indian Institute of Technology Bombay (IITB) with funding from Indo-US Science and Technology Forum and the Science and Engineering Research Board, Department of Science and Technology, Government of India. It is located at the Indian Astronomical Observatory (IAO, Hanle). We acknowledge funding by the IITB alumni batch of 1994, which partially supports the operation of the telescope. Telescope technical details are available at GROWTH-India website <https://sites.google.com/view/growthindia/>.

References

- Afsariardchi, N., Drout, M. R., Khatami, D. K., et al. 2021, *ApJ*, 918, 89
- Anderson, J. P., & James, P. A. 2008, *MNRAS*, 390, 1527
- Aramyan, L. S., Hakobyan, A. A., Petrosian, A. R., et al. 2016, *MNRAS*, 459, 3130
- Arnett, W. D. 1982, *ApJ*, 253, 785
- Bellm, E. C., Kulkarni, S. R., Graham, M. J., et al. 2019, *PASP*, 131, 018002
- Bianco, F. B., Modjaz, M., Hicken, M., et al. 2014, *ApJS*, 213, 19
- Bottinelli, L., Gouguenheim, L., Paturel, G., & de Vaucouleurs, G. 1984, *A&AS*, 56, 381
- . 1985, *A&AS*, 59, 43
- Bottinelli, L., Gouguenheim, L., Paturel, G., & Teerikorpi, P. 1986, *A&A*, 156, 157
- Cano, Z. 2013, *MNRAS*, 434, 1098
- Cano, Z., Maeda, K., & Schulze, S. 2014, *MNRAS*, 438, 2924
- Cao, Y., Kasliwal, M. M., Arcavi, I., et al. 2013, *ApJL*, 775, L7
- Cardelli, J. A., Clayton, G. C., & Mathis, J. S. 1989, *ApJ*, 345, 245
- Castor, J. I., Abbott, D. C., & Klein, R. I. 1975, *ApJ*, 195, 157
- Chambers, K. C., Magnier, E. A., Metcalfe, N., et al. 2016,

Table 1. Log of NIR photometry of SN 2023dbc obtained with kSIRIUS.

MJD	J	err(J)	H	err(H)	K_s	err(K_s)
60018.6	15.209	0.011	14.795	0.022	14.463	0.030
60022.6	14.546	0.012	14.083	0.028	13.746	0.025
60031.5	14.039	0.007	13.692	0.017	13.288	0.013
60036.5	14.077	0.006	13.747	0.012	13.279	0.008
60042.6	14.384	0.008	13.911	0.019	13.528	0.011
60043.6	14.447	0.009	13.988	0.026	13.552	0.009
60047.7	14.721	0.009	14.239	0.015	13.698	0.013
60051.6	14.929	0.013	14.346	0.014	13.901	0.018
60055.6	15.137	0.018	14.476	0.026	14.003	0.039
60056.6	15.050	0.015	14.398	0.018	13.873	0.019
60060.6	15.266	0.012	14.588	0.023	14.112	0.015
60065.6	15.425	0.016	14.444	0.022	14.010	0.021
60073.5	15.696	0.015	14.902	0.016	14.365	0.026
60079.5	15.684	0.031	14.997	0.030	14.458	0.033
60080.5	15.874	0.020	15.104	0.025	14.557	0.026
60087.5	16.139	0.022	15.223	0.025	14.727	0.025

Table 2. Log of optical photometry of SN 2023dbc obtained with ZTF and GIT.

MJD	g	err(g)	r	err(r)	i	err(i)	z	err(z)	Telescope
60020.3	19.263	0.103	17.358	0.039	ZTF
60022.7	17.104	0.025	17.104	0.025	15.723	0.080	GIT
60025.6	18.750	0.051	15.528	0.048	GIT
60030.7	18.688	0.043	16.915	0.034	15.348	0.064	GIT
60036.3	19.017	0.114	16.931	0.047	ZTF
60041.8	17.483	0.050	17.483	0.050	15.757	0.059	GIT
60043.4	17.541	0.041	ZTF
60045.5	20.507	0.231	17.767	0.054	15.955	0.083	GIT
60047.9	17.425	0.040	17.425	0.040	16.114	0.096	GIT
60049.2	17.995	0.067	ZTF
60051.3	18.091	0.070	ZTF
60053.2	18.175	0.067	ZTF
60055.2	18.206	0.063	ZTF
60059.2	18.395	0.064	ZTF
60061.2	18.398	0.071	ZTF
60065.2	18.432	0.071	ZTF
60076.3	18.769	0.090	ZTF
60078.3	18.823	0.097	ZTF
60084.2	18.948	0.105	ZTF
60086.2	18.884	0.137	ZTF
60090.2	18.896	0.110	ZTF
60092.3	19.283	0.111	ZTF
60105.3	19.447	0.129	ZTF

- arXiv e-prints, arXiv:1612.05560
- Cutri, R. M., Skrutskie, M. F., van Dyk, S., et al. 2003, *VizieR Online Data Catalog*, II/246
- de Vaucouleurs, G., Peters, W. L., Bottinelli, L., Gouguenheim, L., & Paturel, G. 1981, *ApJ*, 248, 408
- Dessart, L., Hillier, D. J., Li, C., & Woosley, S. 2012, *MNRAS*, 424, 2139
- Dessart, L., Yoon, S.-C., Aguilera-Dena, D. R., & Langer, N. 2020, *A&A*, 642, A106
- Ergon, M., Sollerman, J., Fraser, M., et al. 2014, *A&A*, 562, A17
- Filippenko, A. V. 1997, *ARA&A*, 35, 309
- Foley, R. J., Papenkova, M. S., Swift, B. J., et al. 2003, *PASP*, 115, 1220
- Fukugita, M., Ichikawa, T., Gunn, J. E., et al. 1996, *AJ*, 111, 1748
- Galama, T. J., Vreeswijk, P. M., van Paradijs, J., et al. 1998, *Nature*, 395, 670
- Giraud, E. 1985, *A&A*, 153, 125
- Graur, O., Bianco, F. B., Modjaz, M., et al. 2017, *ApJ*, 837, 121
- Groh, J. H., Georgy, C., & Ekström, S. 2013, *A&A*, 558, L1
- Hachinger, S., Mazzali, P. A., Taubenberger, S., et al. 2012, *MNRAS*, 422, 70
- Hakobyan, A. A., Mamon, G. A., Petrosian, A. R., Kunth, D., & Turatto, M. 2009, *A&A*, 508, 1259
- Harutyunyan, A. H., Pfahler, P., Pastorello, A., et al. 2008, *A&A*, 488, 383
- Ho, A. Y. Q. 2023, *Transient Name Server Discovery Report*, 2023-533, 1
- Hunter, D. J., Valenti, S., Kotak, R., et al. 2009, *A&A*, 508, 371
- Iwamoto, K., Mazzali, P. A., Nomoto, K., et al. 1998, *Nature*, 395, 672
- Iwamoto, K., Nakamura, T., Nomoto, K., et al. 2000, *ApJ*, 534, 660
- Jencson, J. E., Kasliwal, M. M., Johansson, J., et al. 2017, *ApJ*, 837, 167
- Jencson, J. E., Kasliwal, M. M., Adams, S. M., et al. 2018, *ApJ*, 863, 20
- Kankare, E., Fraser, M., Ryder, S., et al. 2014a, *A&A*, 572, A75
- Kankare, E., Mattila, S., Ryder, S., et al. 2014b, *MNRAS*, 440, 1052
- Kankare, E., Efstathiou, A., Kotak, R., et al. 2021, *A&A*, 649, A134
- Karachentsev, I. D., Kudrya, Y. N., Karachentseva, V. E., & Mitronova, S. N. 2006, *Astrophysics*, 49, 450
- Karachentsev, I. D., Makarov, D. I., & Kaisina, E. I. 2013, *AJ*, 145, 101
- Kashibadze, O. G. 2008, *Astrophysics*, 51, 336
- Kilpatrick, C. D., Takaro, T., Foley, R. J., et al. 2018, *MNRAS*, 480, 2072
- Kinugasa, K., Kawakita, H., Ayani, K., et al. 2002, *ApJL*, 577, L97
- Kool, E. C., Ryder, S., Kankare, E., et al. 2018, *MNRAS*, 473, 5641
- Kumar, H., Bhalerao, V., Anupama, G. C., et al. 2022, *AJ*, 164, 90
- Li, L., Zhai, Q., Zhang, J., & Wang, X. 2023, *Transient Name Server Classification Report*, 2023-559, 1
- Li, W., Leaman, J., Chornock, R., et al. 2011, *MNRAS*, 412, 1441
- Lyman, J. D., Bersier, D., & James, P. A. 2014, *MNRAS*, 437, 3848
- Lyman, J. D., Bersier, D., James, P. A., et al. 2016, *MNRAS*, 457, 328
- Ma, X., Wang, X., Mo, J., et al. 2025, *A&A*, 698, A305
- Maeda, K., Mazzali, P. A., Deng, J., et al. 2003, *ApJ*, 593, 931
- Maeda, K., Kawabata, K., Mazzali, P. A., et al. 2008, *Science*, 319, 1220
- Malesani, D., Tagliaferri, G., Chincarini, G., et al. 2004, *ApJL*, 609, L5
- Marion, G. H., Vinko, J., Kirshner, R. P., et al. 2014, *ApJ*, 781, 69
- Mattila, S., Dahlen, T., Efstathiou, A., et al. 2012, *ApJ*, 756, 111
- Mazzali, P. A., Deng, J., Maeda, K., et al. 2002, *ApJL*, 572, L61
- Mazzali, P. A., Deng, J., Tominaga, N., et al. 2003, *ApJL*, 599, L95
- Mazzali, P. A., Kawabata, K. S., Maeda, K., et al. 2007, *ApJ*, 670, 592
- Modjaz, M., Li, W., Butler, N., et al. 2009, *ApJ*, 702, 226
- Nagayama, T., & Nakaya, H. 2024, in *Society of Photo-Optical Instrumentation Engineers (SPIE) Conference Series*, Vol. 13096, *Ground-based and Airborne Instrumentation for Astronomy X*, ed. J. J. Bryant, K. Motohara, & J. R. D. Vernet, 130963I
- Nasonova, O. G., de Freitas Pacheco, J. A., & Karachentsev, I. D. 2011, *A&A*, 532, A104
- Nomoto, K., Yamaoka, H., Pols, O. R., et al. 1994, *Nature*, 371, 227
- Pastorello, A., Kasliwal, M. M., Crockett, R. M., et al. 2008, *MNRAS*, 389, 955
- Perley, D., Qin, Y., Sharma, Y., & Sollerman, J. 2023, *Transient Name Server Classification Report*, 2023-607, 1
- Prentice, S. J., Mazzali, P. A., Pian, E., et al. 2016, *MNRAS*, 458, 2973
- Sahu, D. K., Anupama, G. C., & Chakradhari, N. K. 2013, *MNRAS*, 433, 2
- Sahu, D. K., Gurugubelli, U. K., Anupama, G. C., & Nomoto, K. 2011, *MNRAS*, 413, 2583
- Schlafly, E. F., & Finkbeiner, D. P. 2011, *ApJ*, 737, 103
- Shingles, L., Smith, K. W., Young, D. R., et al. 2021, *Transient Name Server AstroNote*, 7, 1
- Smith, K. W., Smartt, S. J., Young, D. R., et al. 2020, *PASP*, 132, 085002
- Sorce, J. G., Tully, R. B., Courtois, H. M., et al. 2014a, *MNRAS*, 444, 527
- . 2014b, *MNRAS*, 444, 527
- Springob, C. M., Haynes, M. P., Giovanelli, R., & Kent, B. R. 2005, *ApJS*, 160, 149
- Springob, C. M., Masters, K. L., Haynes, M. P., Giovanelli, R., & Marinoni, C. 2009, *ApJS*, 182, 474
- Stanek, K. Z., Matheson, T., Garnavich, P. M., et al. 2003,

- ApJL, 591, L17
- Stoppa, F., & Smartt, S. J. 2026, arXiv e-prints, arXiv:2603.28741
- Stritzinger, M., Mazzali, P., Phillips, M. M., et al. 2009, ApJ, 696, 713
- Sugimoto, D., & Nomoto, K. 1980, Space Sci. Rev., 25, 155
- Takaki, K., Kawabata, K. S., Yamanaka, M., et al. 2013, ApJL, 772, L17
- Tanaka, M., Yamanaka, M., Maeda, K., et al. 2009a, ApJ, 700, 1680
- Tanaka, M., Tominaga, N., Nomoto, K., et al. 2009b, ApJ, 692, 1131
- Tauris, T. M., Langer, N., & Podsiadlowski, P. 2015, MNRAS, 451, 2123
- Tomita, H., Deng, J., Maeda, K., et al. 2006, ApJ, 644, 400
- Tonry, J. L., Denneau, L., Heinze, A. N., et al. 2018, PASP, 130, 064505
- Tully, R. B., Courtois, H. M., & Sorce, J. G. 2016, AJ, 152, 50
- Tully, R. B., & Fisher, J. R. 1988, Catalog of Nearby Galaxies
- Tully, R. B., Rizzi, L., Shaya, E. J., et al. 2009, AJ, 138, 323
- Tully, R. B., Shaya, E. J., & Pierce, M. J. 1992, ApJS, 80, 479
- Tully, R. B., Courtois, H. M., Dolphin, A. E., et al. 2013, AJ, 146, 86
- Turatto, M., Mazzali, P. A., Young, T. R., et al. 1998, ApJL, 498, L129
- Valenti, S., Benetti, S., Cappellaro, E., et al. 2008a, MNRAS, 383, 1485
- Valenti, S., Elias-Rosa, N., Taubenberger, S., et al. 2008b, ApJL, 673, L155
- Valenti, S., Fraser, M., Benetti, S., et al. 2011, MNRAS, 416, 3138
- Woosley, S. E., Langer, N., & Weaver, T. A. 1995, ApJ, 448, 315
- Yaron, O., & Gal-Yam, A. 2012, PASP, 124, 668
- Yoon, S. C., Woosley, S. E., & Langer, N. 2010, ApJ, 725, 940
- Yoshii, Y., Tomita, H., Kobayashi, Y., et al. 2003, ApJ, 592, 467
- Zampieri, L., Pastorello, A., Turatto, M., et al. 2003, MNRAS, 338, 711
- Zhao, Y.-H., Sun, N.-C., Wu, J., et al. 2025, ApJL, 980, L6